Nano Energy (2015) 15, 453–461

Available online at www.sciencedirect.com

ScienceDirect

journal homepage: www.elsevier.com/locate/nanoenergy

Enhancing sodium-ion battery performance with interlayer-expanded MoS_2-PEO nanocomposites

Yifei Li[a], Yanliang Liang[a], Francisco C. Robles Hernandez[b], Hyun Deog Yoo[a], Qinyou An[a], Yan Yao[a,c,*]

[a]Department of Electrical and Computer Engineering and Materials Science and Engineering Program, University of Houston, Houston, TX 77204, USA
[b]College of Technology, University of Houston, Houston, TX 77204, USA
[c]Texas Center for Superconductivity, University of Houston, Houston, TX 77204, USA

Received 11 April 2015; received in revised form 9 May 2015; accepted 12 May 2015
Available online 21 May 2015

KEYWORDS
PEO-MoS_2;
Interlayer spacing;
Electrochemical performance;
Sodium-ion battery

Abstract
The larger ionic radius of Na ion (1.06 Å) compared with that of Li ion (0.76 Å) is a fundamental reason for the inferior diffusion kinetics of Na ion in intercalation hosts. Here we report interlayer expansion of intercalation hosts as a general strategy to facilitate the solid-state diffusion of Na ions. Based on this strategy, poly(ethylene oxide)-intercalated MoS_2 composites (PEO-MoS_2) were synthesized via a facile exfoliation-restacking method and tested as anode materials for Na-ion batteries (NIBs). The interlayer spacing of MoS_2 was increased from 0.615 nm to 1.45 nm by insertion of controlled amounts of PEO. The bilayer PEO-intercalated MoS_2 composite (PEO_{2L}-MoS_2) exhibits a specific capacity of 225 mA h g^{-1} under a current density of 50 mA g^{-1}, twice as high as that of commercial MoS_2 (com-MoS_2), and shows improved rate performance due to enhanced Na-ion diffusivity. The improvement in the electrochemical performance demonstrates that interlayer expansion is an effective strategy for the development of high performance electrode materials for battery technologies based on the storage of large ions.
Published by Elsevier Ltd.

Introduction

Lithium-ion batteries (LIBs) with their high energy density have been widely applied in electronic devices and electric vehicles [1,2], but the use of lithium is plagued by high cost and limited resource [3]. Sodium, the low-cost and resource

*Corresponding author at: Department of Electrical and Computer Engineering and Materials Science and Engineering Program, University of Houston, Houston, TX 77204, USA.
E-mail address: yyao4@uh.edu (Y. Yao).

http://dx.doi.org/10.1016/j.nanoen.2015.05.012
2211-2855/Published by Elsevier Ltd.

abundant sibling of lithium, shares similar intercalation chemistry with lithium in various intercalation hosts and is expected to enable Na-ion batteries (NIBs) as a more robust version of LIBs [4-7]. One major difference of NIBs from LIBs is the larger ionic radius of Na ion (1.06 Å) than that of Li ion (0.76 Å), which may weaken the advantages of NIBs in terms of the lower volumetric energy density, inferior cycling stability, and even higher ion diffusion barrier in the electrode materials [8-10].

Various intercalation hosts well-established for LIBs were examined as electrode materials for NIBs including layered sulfides MS_2 (M=transition metals) [11-13], layered oxides A_xMO_y (A=Li, Na) [14,15], V_2O_5 [16], olivine A_xFePO_4 (A=Li, Na) [17], conversion ($NiCo_2O_4$, Sb_2O_4 and Co_3O_4) [18-20] and alloying (Sb, Sn and SnO_2) [21-24] reactions based materials [25]. It was found that most of these materials tended to suffer from lower capacity, inferior stability, large volume change and undergo more intermediate phases compared to their LIB counterparts. Therefore, it still remains promising for developing Na intercalation materials if the issue of steric hindrance is addressed.

The inferior kinetics and stability of Na ion storage materials are resulted from the unfavorable compatibility between large intercalating ion and sterically hindered lattice space in host materials. We envision that an increase in lattice spacing of host materials will provide a solution for large-ion storage. Indeed, improved diffusion kinetics was predicted for Li in interlayer-expanded MoS_2 [26]. Our hypothesis is further supported by some recent studies that the intercalation capacity for Na storage was increased largely in V_2O_5 xerogel [27] and expanded graphite [28], both of which have enlarged interlayer spacing, and our recent study that the Mg storage kinetics and stability in MoS_2 were improved significantly with progressively expanded interlayer spacing [29]. A very recent study showed that graphene-like MoS_2 nanoflowers with expanded interlayers (d=0.67 nm compared to the original 0.62 nm) increased Na storage capacity compared with bulk MoS_2 (d=0.62 nm). Although the performance enhancement contributed by reduced particle size and crystallinity was not clearly distinguished from that originated from increased interlayer spacing [30]. We aim to establish a direct relationship between the Na storage behavior and the interlayer spacing of the host without the contributions from other parameters.

Herein we report interlayer expansion as a general material design strategy for layered hosts to tackle the kinetic challenges related to large intercalating cations (e.g. Na ion). MoS_2 is chosen as the model host for its proven versatile structure for ion intercalation [29,31-34]. Importantly, the interlayer distance of MoS_2 can be tuned in a wide range by inserting a controlled amount of guest species to form intercalation compounds [35,36]. This allows a systematic study of the influence of interlayer distance on electrode performance. In this study, poly(ethylene oxide) (PEO) is chosen as the intercalating agent because of its cation-conducting property [37,38]. In addition, PEO-MoS_2 has well-known tunability of the interlayer distance in intercalation composites resulting in lattice expansions up to 160% [39]. We have synthesized PEO-MoS_2 nanocomposites via a facile exfoliation-restacking method. By optimizing the amount of PEO during the synthesis, PEO_{1L}-MoS_2 and PEO_{2L}-MoS_2 containing one and two layers of PEO between two slabs of MoS_2 were achieved, respectively. To make a systematic comparison, commercial MoS_2 (com-MoS_2), restacked MoS_2 (re-MoS_2) without PEO, and the two PEO-MoS_2 nanocomposites were all tested as NIB anode electrodes. The three composites shared similar morphologies and crystallinity, hence allowing for an unambiguous correlation of interlayer spacing to the capacity of Na storage, cycling stability and ion diffusivity. We found the enlargement of the interlayer spacing increased the diffusivity of Na-ion by up to two orders of magnitude, resulting in more than doubled capacity (225 vs 113 mA h g^{-1}) as well as improved rate capability and cycling stability.

Experimental

Preparation of re-MoS_2 and PEO-MoS_2 nanocomposites

Commercially available MoS_2 (2 g) was put into *n*-butyllithium (2.5 M, 12.5 mL) in Schlenk flask inside an Ar-filled glovebox and stirred overnight at room temperature. The mixture was filtrated, washed with hexane for three times, and dried under vacuum at room temperature to form lithiated MoS_2 ($LiMoS_2$). $LiMoS_2$ (2 g) was poured into deionized water (200 mL) and the mixture was sonicated for 1 h and stirred for another 3 h to form a colloid. PEO-MoS_2 composites were obtained by mixing 0.07 and 0.27 g of PEO (Aldrich, M_v=100,000 Da) in H_2O (100 mL) with the MoS_2 colloid (100 mL) to afford PEO_{1L}-MoS_2 and PEO_{2L}-MoS_2, respectively. The re-MoS_2 and PEO-MoS_2 composites were obtained by centrifugation, washing with deionized water for three times, and freeze-drying.

Characterizations

X-ray diffraction (XRD) measurement was performed on a Rigaku MiniFlex 600 with Cu Kα radiation (λ=1.5406 Å). Scanning electron microscopy (SEM) images were collected with Gemini LEO 1525 microscopy. Transmission electron microscopy images (TEM) were recorded using a JEOL 2100 F. Weight percentage of PEO in PEO-MoS_2 composites was calculated by thermogravimetric analysis (TGA) using a thermogravimetric analyzer of TA instruments Q50. X-ray photoelectron spectroscopy (XPS) was measured by a Physical Electronics Model 5700 XPS instrument. The electrochemical properties were tested by assembling CR2032 coin cells in an Ar-filled glove box with sodium metal as the anode and 1 M sodium trifluoromethanesulfonate ($NaCF_3SO_3$) in diethyleneglycol dimethylether (DEGDME) (Sigma Aldrich, anhydrous) as electrolyte. The working electrodes consisted of 70 wt% of active material, 20 wt% of Super-P carbon, and 10 wt% of polyvinylidene fluoride (PVDF). The above materials were mixed in *N*-methyl-2-pyrrolidone, and the resulted slurry was spread on stainless steel foil and dried at 75 °C in vacuum for 10 h. Typical loading of the active materials is about 1.0 mg cm^{-2}. Galvanostatic tests were conducted on a battery testing system (LAND CT2001A). Cyclic voltammetry (CV) and galvanostatic intermittent titration technique (GITT) were measured on an electrochemical workstation (EC-Lab VMP3). Specific capacity was calculated based on the weight of MoS_2.

Results and discussion

As illustrated in Fig. 1, re-MoS_2 and PEO-MoS_2 composites were synthesized based on a facile restacking strategy, which has been described in literature [39]. $LiMoS_2$ was first synthesized from com-MoS_2 by lithiation with *n*-butylithium. When poured into deionized water, $LiMoS_2$ was oxidized by H_2O, leading to exfoliation of the bulk $LiMoS_2$ into single MoS_2 layers. Direct washing and drying formed re-MoS_2. By adding the single-layered MoS_2 suspension to a PEO solution, PEO molecules will adsorb on the surface of MoS_2 layers. After washing and drying, composites containing different amount of PEO in-between MoS_2 layers were obtained. The reaction equations are as follows:

$$Li_xMoS_2 + yH_2O \rightarrow Li_{(x-y)}MoS_2 + yLiOH + y/2H_2 \quad (1)$$

$$Li_{(x-y)}MoS_2 + zPEO \rightarrow Li_{(x-y)}MoS_2(PEO)_z \quad (2)$$

To compare the crystal structure of com-MoS_2, re-MoS_2, PEO_{1L}-MoS_2 and PEO_{2L}-MoS_2, XRD analyses were conducted. As shown in Fig. 2a, the diffraction peak located at 14.4° for com-MoS_2 is implicative of the interlayer distance of MoS_2 along the *c*-axis, which is 0.615 nm. After the exfoliation-restack process, the corresponding peak for re-MoS_2 becomes broadened and weakened in intensity, suggesting a less ordered structure of re-MoS_2. The peak position also slightly shifts to a lower angle of 13.97°, corresponding to a larger interlayer distance of 0.633 nm. With a small amount of PEO intercalated, the distance is increased to 1.19 nm, which is further enlarged to 1.45 nm with the insertion of more PEO. The distances of 1.19 and 1.45 nm respectively correspond to mono- and bilayer PEO intercalation according to the literature [39,40]. PEO_{2L}-MoS_2 exhibits three well-defined peaks at 6.1°, 12.2° and 18.3°, corresponding to the (0 0 1), (0 0 2) and (0 0 3) reflections, respectively. In the case of PEO_{1L}-MoS_2, due to a smaller interlayer spacing compared with PEO_{2L}-MoS_2, the (0 0 1), (0 0 2), and (0 0 3) reflection peaks shift to larger angles of 7.4°, 14.9°, and 22.7° (the latter falls out of the angle range shown in Fig. 2a). Note that several different ratios of PEO have been tried to obtain various interlayer distances, but only two distances that we have reported in this work could be obtained. The addition of more than 0.27 g of PEO cannot generate an interlayer distance larger than the 1.45 nm in PEO_{2L}-MoS_2, and a mass between 0.07 and 0.27 g cannot generate an interlayer spacing between 1.19 and 1.45 nm either, which are consistent with literature results [40]. This may be due to the fact that PEO only exists between MoS_2 layers as mono- or bi-layer fillers, leaving the excess amount of PEO washed away by water.

TGA analysis of re-MoS_2, PEO_{1L}-MoS_2 and PEO_{2L}-MoS_2 are shown in Fig. 2b. The weight loss profile for re-MoS_2 is characterized by a gradual loss between room temperature and 100 °C, followed by a steep loss until 350 °C, corresponding to the loss of 0.21 mol of adsorption water and 1.48 mol of structural water per mole of MoS_2, respectively. PEO_{1L}-MoS_2 and PEO_{2L}-MoS_2 respectively show 9.3 wt% and 21.0 wt% of weight loss due to the decomposition of PEO. The XPS data in Fig. 2d reveals the phase composition of the four samples. For com-MoS_2, the peaks at 232.3, 229.1, 163.1 and 161.9 eV correspond to Mo $3d_{3/2}$, Mo $3d_{5/2}$, S $2p_{1/2}$ and S $2p_{3/2}$ components of 2H MoS_2, where Mo is coordinated to six S atoms in a trigonal prismatic geometry (Fig. 2c). For re-MoS_2, additional Mo 3d peaks at 228.5 eV and 231.65 eV appear, and S 2p spectra also shows additional S $2p_{3/2}$ and S $2p_{1/2}$ peaks. All new peaks from Mo 3d and S 2p spectra can be attributed to 1T MoS_2, where Mo is octahedrally coordinated to S atoms (Fig. 2c) [41]. Therefore, re-MoS_2 contains both 2H and 1T phases. Similarly, for PEO_{1L}-MoS_2 and PEO_{2L}-MoS_2, new peaks for 1T MoS_2 are observed, indicating that PEO intercalation does not alter the phase composition of the restacked MoS_2.

Fig. 3a–d show the SEM images of com-MoS_2, re-MoS_2, PEO_{1L}-MoS_2 and PEO_{2L}-MoS_2. There is significant difference between com-MoS_2 and three synthesized composites. While com-MoS_2 is composed of particles with the diameter of a few micrometers, re-MoS_2, PEO_{1L}-MoS_2 and PEO_{2L}-MoS_2 exhibit two-dimensional laminar structures with more than 20 μm in size. Fig. 3e–h shows the high-resolution TEM (HRTEM) images of the four samples where the interlayer

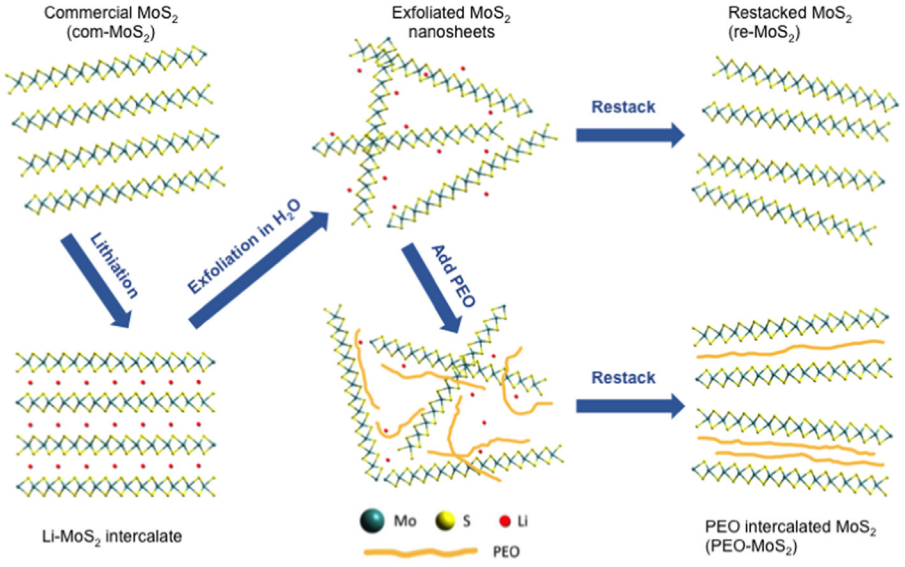

Fig. 1 Schematic diagram of synthesis of restacked MoS_2 (re-MoS_2) and PEO-MoS_2 via exfoliation-restacking process.

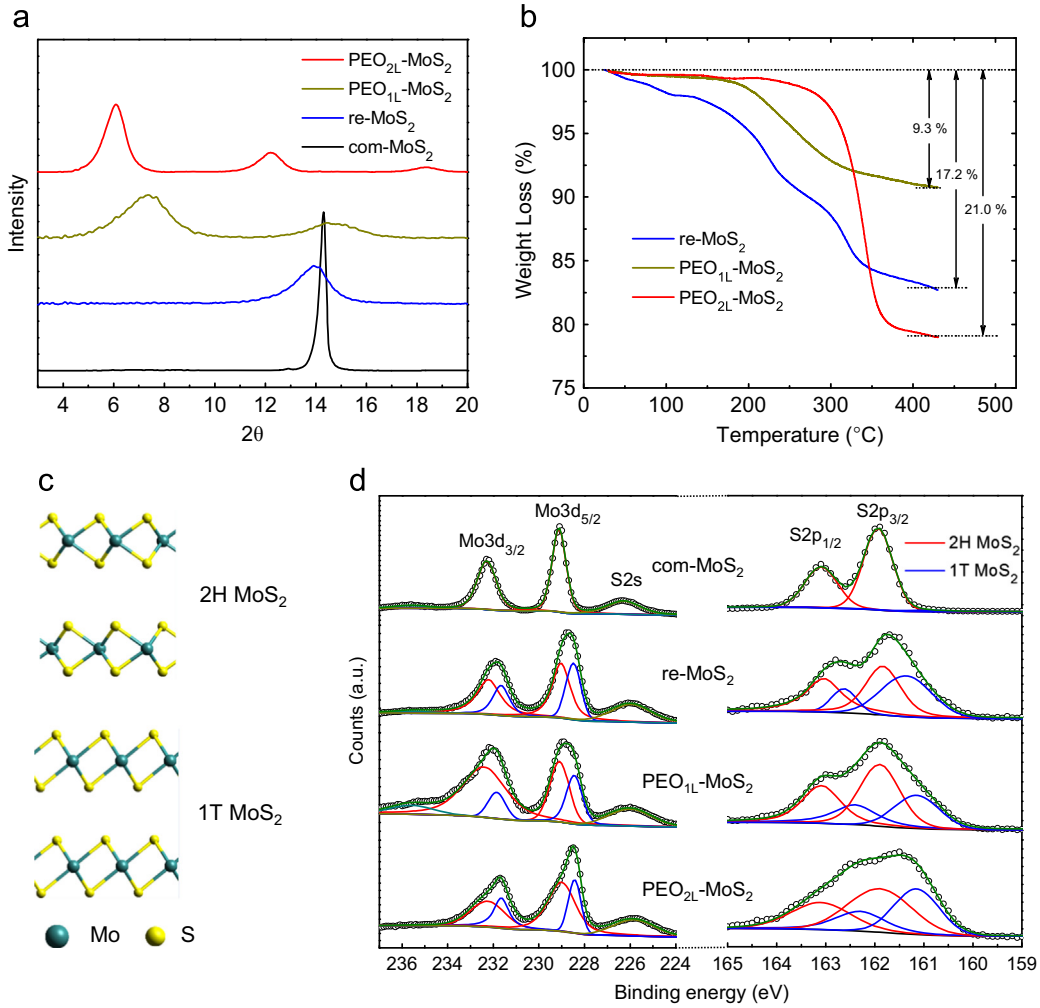

Fig. 2 (a) XRD and (b) TGA of com-MoS_2, re-MoS_2, PEO_{1L}-MoS_2 and PEO_{2L}-MoS_2. (c) Structure of 2H and 1T phase MoS_2. (d) XPS spectra of Mo 3d, S 2s and S 2p peaks for the four samples. The Mo 3d and S 2p peaks were deconvoluted to show the ratio of 2H and 1T phase MoS_2, represented by red and blue plots, respectively.

distance of MoS_2 along the *c*-axis can be clearly observed. The pristine com-MoS_2 has the most ordered layered structure with the smallest interlayer spacing. The layered structure of re-MoS_2 becomes less ordered and it has slightly increased interlayer distance compared with com-MoS_2, agreeing with the broadened and slightly shifted diffraction peak in XRD spectrum. Both PEO_{1L}-MoS_2 and PEO_{2L}-MoS_2 show less ordered structures and much enlarged interlayer distance (1.1 nm for PEO_{1L}-MoS_2 and 1.4 nm for PEO_{2L}-MoS_2), which are in accordance to those calculated from XRD spectra. Note that the backbone of PEO can be observed in the TEM image for PEO_{1L}-MoS_2 (Fig. 3g, highlighted with yellow arrows), which is a direct evidence of the presence of PEO between MoS_2 layers. The similar morphology, size, and crystallinity for re-MoS_2, PEO_{1L}-MoS_2 and PEO_{2L}-MoS_2 make the interlayer distance the unique variable in contribution to the difference in electrochemical performance.

Fig. 4 displays the CV curves at a scan rate of 0.1 mV s^{-1} and the charge-discharge curves at a current density of 50 mA g^{-1} for the four samples for the first, second, and fifth cycles. Because conversion reaction of MoS_2 starts at 0.4 V vs Na/Na^+ and leads to poor cycling stability [12,30]. The lower cut-off voltage was thus set to 0.4 V. The first-cycle CV curve of com-MoS_2 shows two major sharp reduction peaks at 0.91 and 0.65 V and three oxidation peaks at 1.30, 1.52 and 2.34 V (Fig. 4a), which agrees with the two well-defined plateaus at 0.92 and 0.68 V and the three plateaus at about 1.30, 1.50, and 2.30 V in the charge curve in Fig. S1a. It is known that during lithium-ion intercalation, MoS_2 undergoes a trigonal prismatic (2H)-octahedral (1T) phase transition and displays a well-defined discharge plateau in the first cycle, which fades in subsequent cycles [42,43]. The several CV peaks and plateaus indicate that Na ion storage in MoS_2 shows similar phase transitions but in multiple steps. These stepwise phase transitions are likely due to a staging process, which describes the scenario that certain interlayer regions of MoS_2 are filled with Na ions whereas others are completely vacant [44]. This staging process can help minimize the energy for opening up the vdW gap between layers and is common for layered transition metal sulfides for storage of large ions [44,45]. For example, previous studies on alkaline ion intercalation into TiS_2 show that no staging phenomenon was observed for Li

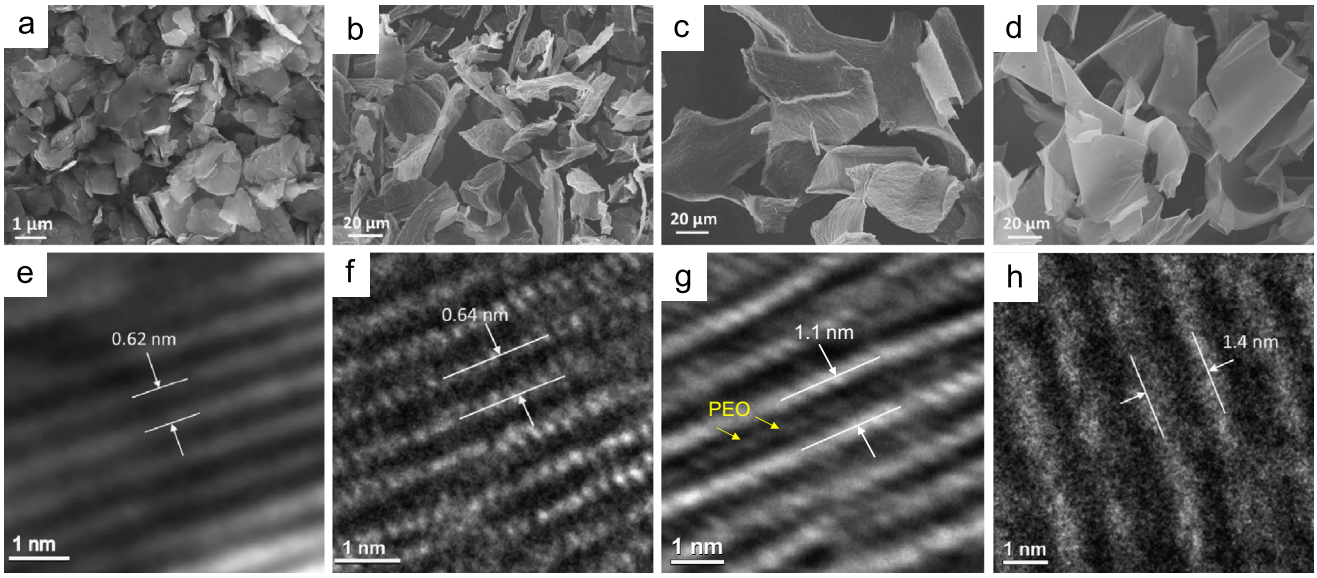

Fig. 3 (a–d) SEM images of the morphology of com-MoS_2, re-MoS_2, PEO_{1L}-MoS_2 and PEO_{2L}-MoS_2. (e–h) HRTEM images show the cross-sectional view of the interlayer spacing in four samples.

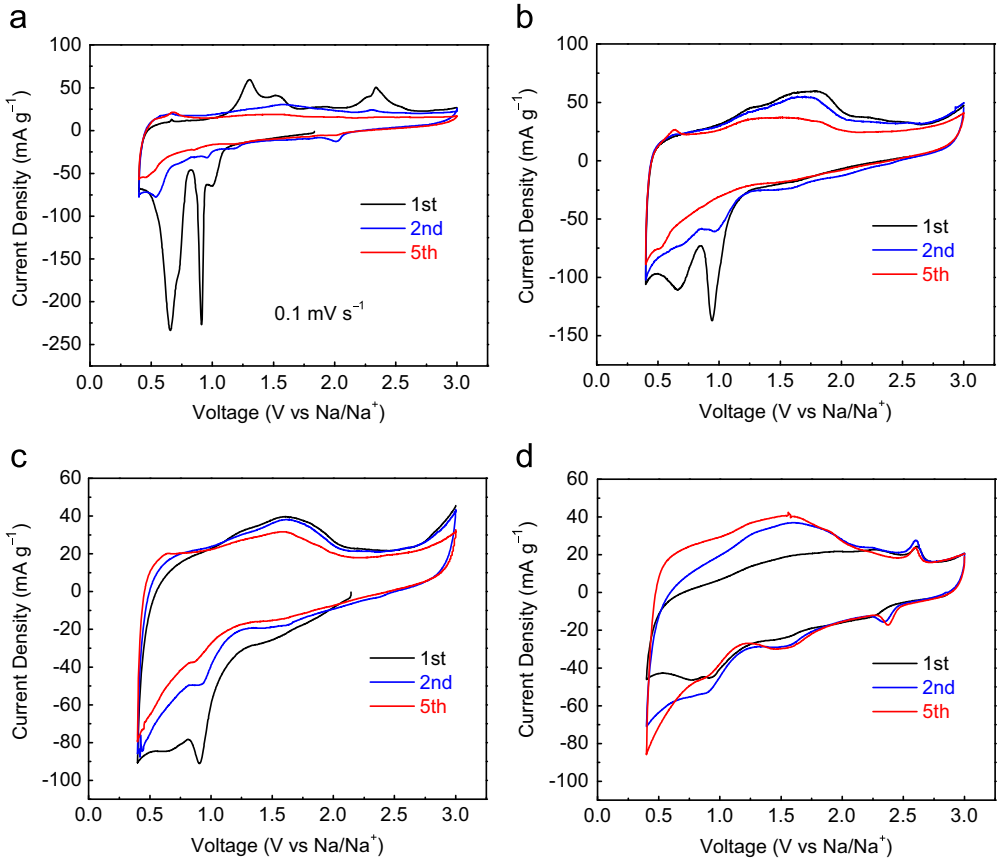

Fig. 4 Cyclic voltammograms of (a) com-MoS_2, (b) re-MoS_2, (c) PEO_{1L}-MoS_2 and (d) PEO_{2L}-MoS_2 with scan rate of 0.1 mV s^{-1} and sodium metal as the counter and reference electrodes at the 1st, 2nd and 5th cycle.

intercalation, while staging was observed for intercalation of larger cations such as Na and K ions [45,46]. The two reduction peaks at 0.95–0.85 and 0.75–0.6 V in the first CV cycle correspond to the phase transitions from pristine MoS_2 to the second-stage compound and then the second- to the first-stage compound, respectively, while the oxidation peaks correspond to the reverse process. These peaks in CV and plateaus in charge–discharge curves become less

obvious and even disappear in the subsequent cycles. This phenomenon is characteristic of irreversible phase transitions as reported in the literature [12]. For re-MoS_2, two cathodic peaks at 0.94 and 0.66 V were observed without well-defined anodic peaks (Fig. 4b). The presence of cathodic peaks indicate that even though the vdW gap between MoS_2 layers has been opened up during the synthesis of re-MoS_2, the restacked layers still require energy to reopen the vdW gap and result in staging during Na intercalation, albeit less evident than that for com-MoS_2. PEO_{1L}-MoS_2 shows even less well-defined peaks in CV (Fig. 4c) compared with re-MoS_2, and PEO_{2L}-MoS_2, for the first cycle, exhibits no well-defined peak at all (Fig. 4d). These behaviors indicate that the insertion of PEO can effectively mitigate the interlayer interaction of MoS_2, thus resulting in minimum energy to open the vdW gap and hence little reliance on a staging process. On the fifth cycle, all four samples show similar CV and voltage profiles (Fig. 5a) with no apparent peaks and plateaus, suggesting that after phase transitions within the initial few cycles, the four samples tend to behave similarly.

Fig. 5b shows the capacity retention of the four samples upon cycling. The initial specific discharge capacity for com-MoS_2 was 242 mA h g^{-1}; however, half capacity was lost after 5 cycles. Structural distortion occurred during the initial irreversible phase transitions should be responsible for the inferior stability [12]. The initial capacity of re-MoS_2 was close to that of com-MoS_2, but 67% of initial capacity was retained after 5 cycles; implying that the larger interlayer spacing of MoS_2 layers makes Na (de)intercalation more reversible.

With further increase in interlayer distance, PEO_{1L}-MoS_2 exhibited better capacity retention than that of re-MoS_2 after the first 10 cycles. From the 10th to the 70th cycle, the capacity for PEO_{1L}-MoS_2 decreased from 141 mA h g^{-1} to 119 mA h g^{-1}, corresponding to 84% capacity retention. PEO_{2L}-MoS_2 with the largest interlayer spacing showed the highest capacity (225 mA h g^{-1}) among the four samples after an initial 5 cycle activation stage and did not show dramatic capacity loss as other samples (148 mA h g^{-1} at the 70th cycle). The improved stability of PEO_{2L}-MoS_2 could be attributed to the absence of a staging process and thus no unfavorable structural distortion. The presence of an activation stage is only observed for PEO_{2L}-MoS_2 presumably because of the combination of the high PEO content in the composite and the high viscosity (0.97 cP) of the DEGDME solvent in the electrolyte. PEO does not only locate between MoS_2 layers but also serves as a glue to connect the layers into large flakes as observed in the SEM images. It takes an additional wetting process for the electrolyte to fully penetrate such polymer glue and access all the electrode material. This process is not obvious for PEO_{1L}-MoS_2 where the amount of PEO is small (44% of that for PEO_{2L}-MoS_2). We also note that the use of the much less viscous tetrahydrofuran (0.55 cP) as the solvent for the electrolyte also eliminates the activation process for PEO_{2L}-MoS_2 (Fig. S2).

When tested at a higher current density of 0.5 A g^{-1}, PEO_{2L}-MoS_2 exhibited Coulombic efficiency of more than 99% after activation and specific capacity of 140 mA h g^{-1} with slow decay (Fig. S3). The rate performance of the four samples is shown in Fig. 5c. The specific capacities of PEO_{2L}-MoS_2 were 185 (after activation), 162, 143, 127 and 112 mA h g^{-1} under current densities of 50, 100, 250, 500 and 1 A g^{-1}, respectively, which are higher than those of other three samples. At 1 A g^{-1}, the capacity for PEO_{2L}-MoS_2 is three times as high as that of com-MoS_2. The enhanced rate performance indicates that expanded interlayer distance can result in faster electrode kinetics.

To investigate the effect of interlayer distance on the diffusivity of Na ion in MoS_2, GITT was employed to probe the diffusivity of Na ion [47,48]. Fig. 6a shows the GITT curve of PEO_{2L}-MoS_2 after activation. During the GITT measurement, the cell was discharged or charged at a current density of 50 mA g^{-1} for 10 min and then rested for 30 min to reach the steady-state voltage (E_s) (Fig. 6b). The Na ion diffusivity D^{GITT} can be obtained via the formula [47],

$$D^{GITT} = \frac{4}{\pi\tau}\left(\frac{m_B V_M}{M_B S}\right)^2\left(\frac{\Delta E_s}{\Delta E_t}\right)^2 \quad (3)$$

where τ denotes the constant current pulse time, m_B, M_B and V_M are the mass, molar weight and molar volume of PEO_{2L}-MoS_2, respectively, S is the area of the electrode-electrolyte interface, ΔE_s is the change of E_s obtained by subtracting the original voltage (E_0) from the steady-state voltage (E_s), and ΔE_τ is the total change of cell voltage during a constant current pulse τ excluding the IR-drop. Fig. 6c shows the plot of Na ion diffusivity as a function of Na ion concentration (x) in Na_xMoS_2 of all four samples during discharge process. At low Na concentration

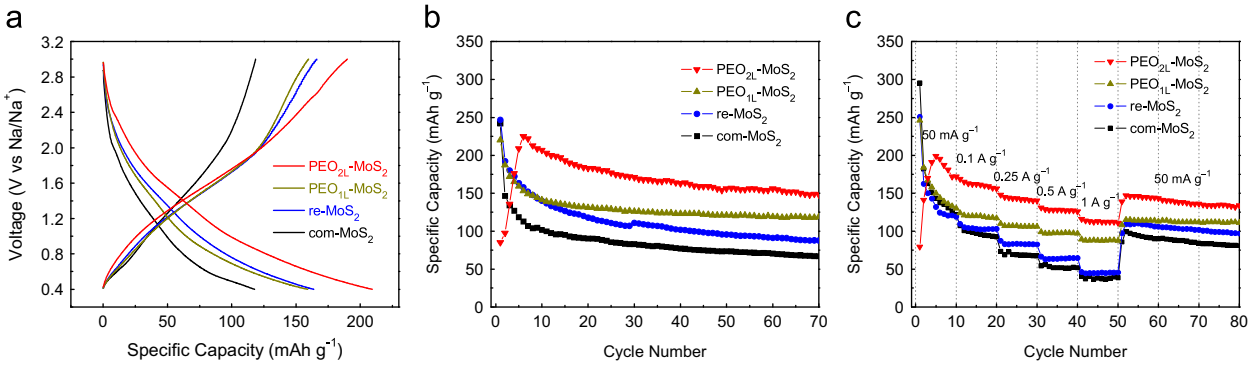

Fig. 5 (a) Galvanostatic charge–discharge voltage profiles of com-MoS_2, re-MoS_2, PEO_{1L}-MoS_2 and PEO_{2L}-MoS_2 at the 5th cycle. (b) Typical cycling behavior at 50 mA g^{-1} and rate performance (c) of these samples.

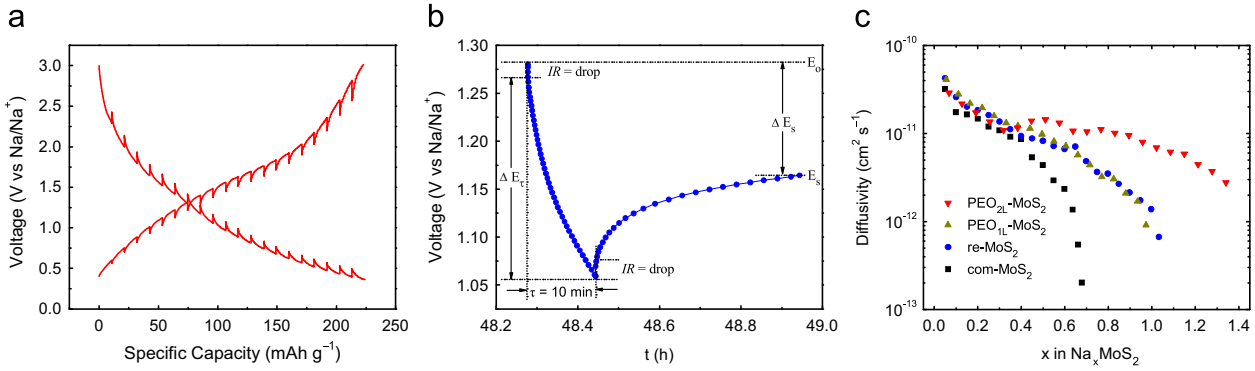

Fig. 6 (a) GITT of a PEO_{2L}-MoS_2 electrode. (b) Voltage-time profile during a GITT measurement around 1.17 V. (c) The plot of Na ion diffusivity as a function of Na concentration in com-MoS_2, re-MoS_2, PEO_{1L}-MoS_2 and PEO_{2L}-MoS_2 samples during discharge process.

($0<x<0.4$), all samples show similar diffusivities of 10^{-10}-10^{-11} $cm^2\ s^{-1}$. Beyond $x=0.4$, the diffusivity for com-MoS_2 drops significantly and finally reaches 2.02×10^{-13} $cm^2\ s^{-1}$ at $x=0.68$, at which point Na intercalation stopped. Diffusivities of both re-MoS_2 and PEO_{1L}-MoS_2 decrease slower than com-MoS_2 and eventually reached 10^{-12} $cm^2\ s^{-1}$ at $x=1.0$. Na ion diffusivity in PEO_{2L}-MoS_2 shows the slowest decrease and is at 2.78×10^{-12} $cm^2\ s^{-1}$ with x being 1.34. Diffusivity measured in the charge process also falls within the range of 10^{-10}-10^{-12} $cm^2\ s^{-1}$, similar to the discharge process (Fig. S4). All these results indicate that interlayer expansion is an effective strategy to improve the diffusion kinetics of Na ion in MoS_2.

Based on the above results, we can conclude that the improvement in electrode performance of MoS_2 for NIBs is the result of expanded interlayer spacing. Our study differs from previous reports in that the samples synthesized herein have similar particle size and crystallinity, allowing for the establishment of an unambiguous relationship between the Na storage behavior and the interlayer spacing of the host. For example, particle-downsizing alone is known to be an effective method to shorten the ion diffusion length in electrode materials and increase the apparent ion diffusivity, therefore it is necessary to exclude the contribution from particle size when the influence of interlayer spacing is studied [49]. Similarly, the degree of crystallinity is another key parameter that makes a considerable difference on the electrochemical behaviors and could obscure conclusions if not properly considered [50]. The similar particle size and crystallinity of our samples equalize the possible influence coming from the two parameters. This makes it possible to prove that it is the expanded interlayer spacing that improves electrode performance. Importantly, our strategy does not seem to be host-specific and could be applied to other hosts. Numerous redox active layered materials have been reported to form interlayer-expanded intercalation compounds with molecules, polymers, clusters and metals [51–54]. Therefore, our strategy will lead to a wide range of interesting electrode materials for large-ion intercalation chemistry.

Conclusions

In summary, PEO-MoS_2 nanocomposites have been synthesized via a facile exfoliation-restacking method to tune the interlayer spacing of MoS_2. They serve as a model compound to demonstrate our interlayer expansion strategy to address the challenges of large-ion intercalation chemistry. Our results show that with the interlayer distance increases, the capacity of MoS_2 increases accordingly. In particular, PEO_{2L}-MoS_2 with a 160% increase in interlayer distance exhibits a specific capacity of 210 mA h g^{-1} under a current density of 50 mA g^{-1}, more than twice as high as that of com-MoS_2, as well as improved rate performance and cycling stability. The increased Na-ion diffusivity in interlayer-expanded MoS_2 is found to be responsible for the improvement in electrode performance. Such interlayer-expanded MoS_2 nanocomposites are promising for the use as anode materials for NIBs. Our interlayer expansion strategy can also be extended to other host materials and pave the way for exploring high performance electrode materials for the storage of large ions.

Acknowledgements

Y.Y. acknowledges the support from the Office of Naval Research (no. N00014-13-1-0543) for interlayer-expanded MoS_2 nanocomposite synthesis and National Science Foundation (CMMI-1400261) for sodium ion battery characterizations. FCRH thanks Rice University for the use of TEM JEOL 2100.

Appendix A. Supporting information

Supplementary data associated with this article can be found in the online version at http://dx.doi.org/10.1016/j.nanoen.2015.05.012.

References

[1] M. Armand, J.M. Tarascon, Nature 451 (2008) 652–657.
[2] J.M. Tarascon, M. Armand, Nature 414 (2001) 359–367.
[3] J.-M. Tarascon, Nat. Chem. 2 (2010) 510.
[4] S.-W. Kim, D.-H. Seo, X. Ma, G. Ceder, K. Kang, Adv. Energy Mater. 2 (2012) 710–721.
[5] M.D. Slater, D. Kim, E. Lee, C.S. Johnson, Adv. Funct. Mater. 23 (2013) 947–958.
[6] H. Pan, Y.-S. Hu, L. Chen, Energy Environ. Sci. 6 (2013) 2338–2360.

[7] D. Kundu, E. Talaie, V. Duffort, L.F. Nazar, Angew. Chem. Int. Ed. 54 (2015) 3431–3448.
[8] V.L. Chevrier, G. Ceder, J. Electrochem. Soc. 158 (2011) A1011–A1014.
[9] S.P. Ong, V.L. Chevrier, G. Hautier, A. Jain, C. Moore, S. Kim, X. Ma, G. Ceder, Energy Environ. Sci. 4 (2011) 3680–3688.
[10] S.Y. Hong, Y. Kim, Y. Park, A. Choi, N.-S. Choi, K.T. Lee, Energy Environ. Sci. 6 (2013) 2067–2081.
[11] K.M. Abraham, Solid State Ionics 7 (1982) 199–212.
[12] J. Park, J.-S. Kim, J.-W. Park, T.-H. Nam, K.-W. Kim, J.-H. Ahn, G. Wang, H.-J. Ahn, Electrochim. Acta 92 (2013) 427–432.
[13] C. Zhu, X. Mu, P.A. van Aken, Y. Yu, J. Maier, Angew. Chem. Int. Ed. 53 (2014) 2152–2156.
[14] A. Mendiboure, C. Delmas, P. Hagenmuller, J. Solid State Chem. 57 (1985) 323–331.
[15] C. Delmas, J.-J. Braconnier, C. Fouassier, P. Hagenmuller, Solid State Ionics 3-4 (1981) 165–169.
[16] S. Tepavcevic, H. Xiong, V.R. Stamenkovic, X. Zuo, M. Balasubramanian, V.B. Prakapenka, C.S. Johnson, T. Rajh, ACS Nano 6 (2011) 530–538.
[17] P. Moreau, D. Guyomard, J. Gaubicher, F. Boucher, Chem. Mater. 22 (2010) 4126–4128.
[18] R. Alcántara, M. Jaraba, P. Lavela, J.L. Tirado, Chem. Mater. 14 (2002) 2847–2848.
[19] Q. Sun, Q.-Q. Ren, H. Li, Z.-W. Fu, Electrochem. Commun. 13 (2011) 1462–1464.
[20] M.M. Rahman, A.M. Glushenkov, T. Ramireddy, Y. Chen, Chem. Commun. 50 (2014) 5057–5060.
[21] M. He, K. Kravchyk, M. Walter, M.V. Kovalenko, Nano Lett. 14 (2014) 1255–1262.
[22] H. Zhu, Z. Jia, Y. Chen, N. Weadock, J. Wan, O. Vaaland, X. Han, T. Li, L. Hu, Nano Lett. 13 (2013) 3093–3100.
[23] X. Xie, K. Kretschmer, J. Zhang, B. Sun, D. Su, G. Wang, Nano Energy 13 (2015) 208–217.
[24] Y. Wang, D. Su, C. Wang, G. Wang, Electrochem. Commun. 29 (2013) 8–11.
[25] C. Bommier, X. Ji, Isr. J. Chem. (2015). http://dx.doi.org/10.1002/ijch.201400118.
[26] Y. Li, D. Wu, Z. Zhou, C.R. Cabrera, Z. Chen, J. Phys. Chem. Lett. 3 (2012) 2221–2227.
[27] Q. Wei, J. Liu, W. Feng, J. Sheng, X. Tian, L. He, Q. An, L. Mai, J. Mater. Chem. A 3 (2015) 8070–8075.
[28] Y. Wen, K. He, Y. Zhu, F. Han, Y. Xu, I. Matsuda, Y. Ishii, J. Cumings, C. Wang, Nat. Commun. 5 (2014) 4033.
[29] Y. Liang, H.D. Yoo, Y. Li, J. Shuai, H.A. Calderon, F.C. Robles Hernandez, L.C. Grabow, Y. Yao, Nano Lett. 15 (2015) 2194–2202.
[30] Z. Hu, L. Wang, K. Zhang, J. Wang, F. Cheng, Z. Tao, J. Chen, Angew. Chem. Int. Ed. 53 (2014) 12794–12798.
[31] H. Liu, D. Su, R. Zhou, B. Sun, G. Wang, S.Z. Qiao, Adv. Energy Mater. 2 (2012) 970–975.
[32] J. Xiao, D. Choi, L. Cosimbescu, P. Koech, J. Liu, J.P. Lemmon, Chem. Mater. 22 (2010) 4522–4524.
[33] R. Wang, C. Xu, J. Sun, Y. Liu, L. Gao, H. Yao, C. Lin, Nano Energy 8 (2014) 183–195.
[34] Y. Liang, R. Feng, S. Yang, H. Ma, J. Liang, J. Chen, Adv. Mater. 23 (2011) 640–643.
[35] W.M.R. Divigalpitiya, R.F. Frindt, S.R. Morrison, Science 246 (1989) 369–371.
[36] E. Benavente, M.A. Santa Ana, F. Mendizábal, G. González, Coord. Chem. Rev. 224 (2002) 87–109.
[37] G. Nagasubramanian, A.I. Attia, G. Halpert, E. Peled, Solid State Ionics 67 (1993) 51–56.
[38] M. Jaipal Reddy, J. Siva Kumar, U.V. Subba Rao, P.P. Chu, Solid State Ionics 177 (2006) 253–256.
[39] G. González, M.A. Santa Ana, E. Benavente, J.P. Donoso, T.J. Bonagamba, N.C. Mello, H. Panepucci, Solid State Ionics 85 (1996) 225–230.
[40] J.P. Lemmon, M.M. Lerner, Chem. Mater. 6 (1994) 207–210.
[41] G. Eda, H. Yamaguchi, D. Voiry, T. Fujita, M. Chen, M. Chhowalla, Nano Lett. 11 (2011) 5111–5116.
[42] L. Wang, Z. Xu, W. Wang, X. Bai, J. Am. Chem. Soc. 136 (2014) 6693–6697.
[43] N. Imanishi, M. Toyoda, Y. Takeda, O. Yamamoto, Solid State Ionics 58 (1992) 333–338.
[44] M.S. Whittingham, A.J. Jacobson, Intercalation Chemistry, Academic, New York, 1982.
[45] A.J. Jacobson, L.F. Nazar, Intercalation Chemistry. Encyclopedia of Inorganic and Bioinorganic Chemistry, John Wiley & Sons, Ltd, 2011.
[46] G.H. Newman, L.P. Klemann, J. Electrochem. Soc. 127 (1980) 2097–2099.
[47] E. Deiss, Electrochim. Acta 50 (2005) 2927–2932.
[48] W. Weppner, R.A. Huggins, J. Electrochem. Soc. 124 (1977) 1569–1578.
[49] A.S. Arico, P. Bruce, B. Scrosati, J.-M. Tarascon, W. van Schalkwijk, Nat. Mater. 4 (2005) 366–377.
[50] T. Shiratsuchi, S. Okada, J. Yamaki, T. Nishida, J. Power Sources 159 (2006) 268–271.
[51] R.R. Chianelli, J.C. Scanlon, M.S. Whittingham, F.R. Gamble, Inorg. Chem. 14 (1975) 1691–1696.
[52] L.F. Nazar, A.J. Jacobson, J. Chem. Soc., Chem. Commun. (1986) 570–571.
[53] M.G. Kanatzidis, C.G. Wu, H.O. Marcy, C.R. Kannewurf, J. Am. Chem. Soc. 111 (1989) 4139–4141.
[54] J.P. Motter, K.J. Koski, Y. Cui, Chem. Mater. 26 (2014) 2313–2317.

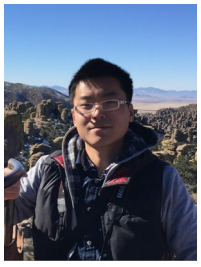

Yifei Li received his B.S. degree from Wuhan University in 2012. He is currently pursuing a Ph.D. in Materials Science and Engineering at the University of Houston in Dr. Yan Yao's group. His research focuses on nanostructured electrode materials for advanced Na-ion and Mg-ion batteries.

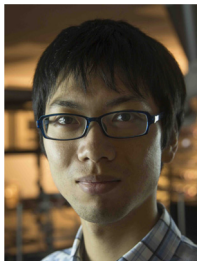

Yanliang Liang received his B.S. in 2007 and Ph.D. in 2012 from Nankai University, China, and is now a postdoctoral fellow in the University of Houston. His research interests are in the development of organic/hybrid materials for energy conversion and storage.

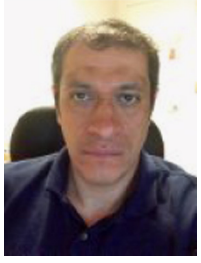

Francisco C. Robles Hernandez received his BS and MS degrees in Metallurgy and Materials Science, respectively. Both degrees were obtained at the Instituto Politécnico Nacional, Mexico in 1996 and 1999. He received his PhD in 2004 from the University of Windsor, Canada. From 2005 to 2008 he worked at the Transportation Technology Center, Inc. as a Senior Scientist/Chief Metallurgist. In 2008 he joined the University of Houston as an Assistant Professor, in 2014 he became a Tenured and Associate Professor. His research interests focus on Nanotechnology, characterization and structural materials (e.g. composites) for a wide variety of applications.

Hyun Deog Yoo received Ph.D. in Chemical and Biological Engineering from Seoul National University in 2011, and then worked as a postdoctoral researcher in Prof. D. Aurbach's lab at Bar-Ilan University from 2011 to 2013. Since 2013, he joined Dr. Yan Yao's group at University of Houston as a postdoctoral researcher. His research interest is the electrochemistry of energy-storing materials including magnesium ion batteries and supercapacitors.

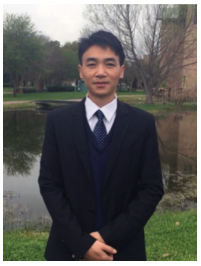

Qinyou An received his Ph.D. in Wuhan University of Technology, and he is presently a postdoctoral fellow in University of Houston. Currently, His research interest covers high energy Li-ion batteries, Na-ion batteries and Mg-ion battery for electric vehicle and large-scale energy storage applications.

Yan Yao received his B.S. and M.S. degrees in Materials Science from Fudan University in 2000 and 2003. He received his Ph.D. in Materials Science and Engineering at University of California, Los Angeles in 2008. He went on to work as a senior scientist at Polyera Corporation and then as a postdoctoral fellow at Stanford University. In 2012, he became an assistant professor at the University of Houston. His research interests focus on magnesium/sodium ion batteries, aqueous batteries, and organic materials for energy storage. He has received the ONR Young Investigator Award (2013), Ralph E. Powe Junior Faculty Enhancement Award (2013) and Robert A. Welch Professorship (2012).